Chapter 13
Fully Packed Loop Models on Finite Geometries

Jan de Gier

13.1 Fully Packed Loop Models on the Square Lattice

A fully packed loop (FPL) model on the square lattice is the statistical ensemble of all loop configurations, where loops are drawn on the bonds of the lattice, and each loop visits every site once [4, 18]. On finite geometries, loops either connect external terminals on the boundary, or form closed circuits, see for example Fig. 13.1. In this chapter we shall be mainly concerned with FPL models on squares and rectangles with an alternating boundary condition where every other boundary terminal is covered by a loop segment, see Fig. 13.1.

An FPL model thus describes the statistics of closely packed polygons on a finite geometry. Polygons may be nested, corresponding to punctures studied in Chapter 8. FPL models can be generalised to include weights. In particular we will study FPL models where a weight τ is given to each straight local loop segment. The partition function of an FPL model on various geometries can be computed exactly using its relation to the solvable six-vertex lattice model. It is well known that the model undergoes a bulk phase transition at $\tau = 2$.

We furthermore study nests of polygons connected to the boundary. In the case of FPL models with mirror or rotational symmetry, the probability distribution function of such nests is known analytically, albeit conjecturally. FPL models undergo another phase transition as a function of the boundary nest fugacity. At criticality, we derive a scaling form for the nest distribution function which displays an unusual non-Gaussian cubic exponential behaviour.

The purpose of this chapter is to collect and discuss known results for FPL models which may be relevant to polygon models. For that reason we have not put an emphasis on derivations, many of which are well-documented in the existing literature, but rather on interpretations of results.

Jan de Gier
Department of Mathematics and Statistics, The University of Melbourne, Victoria, Australia, e-mail: degier@ms.unimelb.edu.au

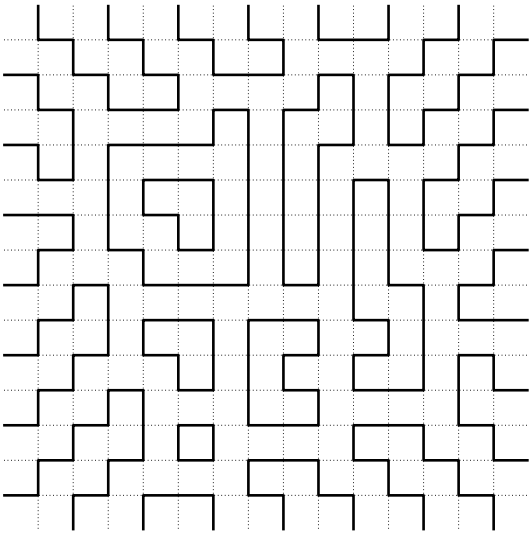

Fig. 13.1 Fully packed loops inside a square with alternating boundary condition.

13.1.1 Bijection with the Six-Vertex Model, Alternating-Sign Matrices and Height Configurations

There is a well-known one-to-one correspondence between FPL, six-vertex and alternating-sign configurations [69, 25]. In the six-vertex model, to each bond of the square lattice is associated an arrow, such that at each vertex there are two in- and two out-pointing arrows, see e.g. [7]. There are six local vertex configurations which are given in the top row of Fig. 13.2. The six-vertex and FPL configurations are related in the following way. The square lattice is divided into two sublattices, even (A) and odd (B). For each arrow configuration we draw only those bonds on which the arrow points to the even sublattice. If we choose the vertex in the upper

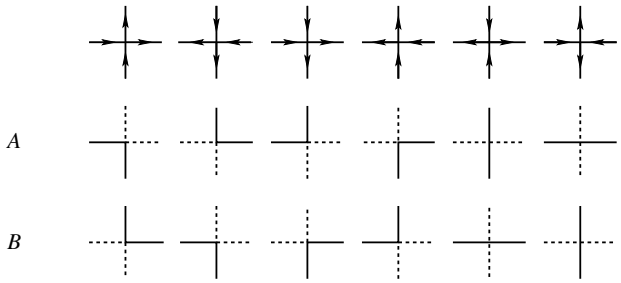

Fig. 13.2 Bijection between six-vertex and FPL vertices. The correspondence is different on the two sublattices A and B.

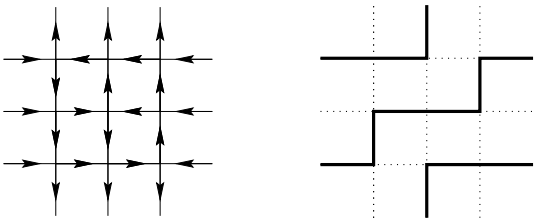

Fig. 13.3 An equivalent six-vertex and fully packed loop configuration.

left corner to belong to the even sublattice, the six-vertex and FPL configuration in Fig. 13.3 are equivalent, as can be seen from the correspondence in Fig. 13.2.

Alternating sign matrices (ASMs) were introduced by Mills, Robbins and Rumsey [51, 52] and are matrices with entries in $\{-1,0,1\}$ such that the entries in each column and each row add up to 1 and the non-zero entries alternate in sign. A well-known subclass of ASMs are the permutation matrices. Let us also introduce the height interpretation of an ASM. Let $A = (a_{ij})_{i,j=1}^{n}$ be an ASM, then define the heights h_{ij} by

$$h_{ij} = n - i - j + 2 \sum_{i' \le i,\ j' \le j} a_{i'j'}. \tag{13.1}$$

This rule ensures that neighbouring heights differ by one. The correspondence between the three objects is given in Fig. 13.4. An example of a six vertex and its corresponding height configuration is given in Fig. 13.5 for the 3×3 identity matrix.

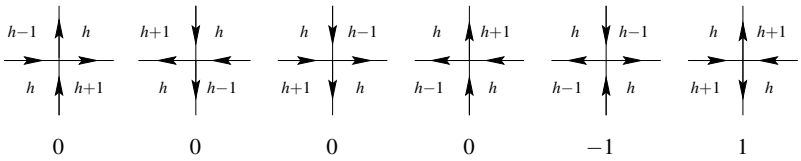

Fig. 13.4 The six vertices and their corresponding heights and ASM entries.

13.1.2 Structure

As each external terminal, or outgoing bond, is connected to another terminal, FPL diagrams can be naturally labeled by link patterns, or equivalently, two-row Young tableaux or Dyck paths. For example, the diagram in Fig. 13.6 has link pattern $((()(()))())$ which is short hand for saying that 1 is connected to 12, 2 is connected to 11, 3 to 4 etc. The information about connectivities can also be coded in two-row standard Young tableaux. The entries of the first row of the Young tableau correspond to the positions of opening parentheses '(' in a link pattern, and the entries of

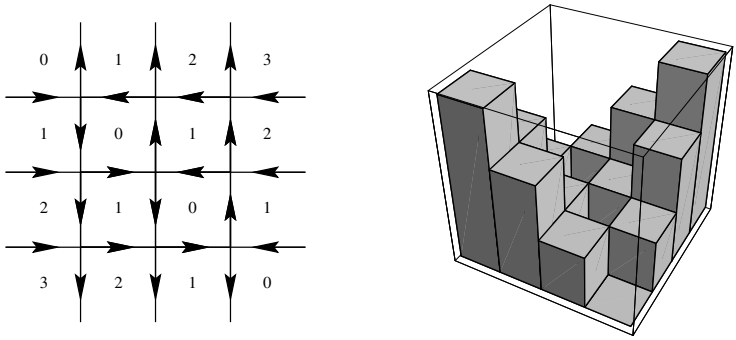

Fig. 13.5 Vertex and height interpretation corresponding to the 3×3 identity matrix.

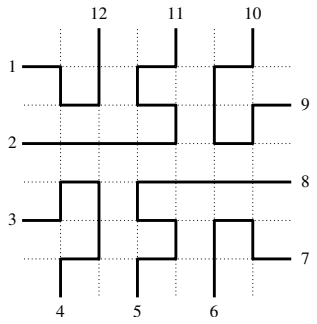

Fig. 13.6 An FPL diagram with link pattern $(((())(()))())$.

the second row to the positions of the closing parentheses ')'. The FPL diagram of Fig. 13.6 carries as a label the standard Young tableau given in Fig. 13.7.

1	2	3	5	6	9
4	7	8	10	11	12

Fig. 13.7 Standard Young tableau corresponding to the FPL diagram in Fig. 13.6.

Yet another way of coding the same information uses Dyck paths. Each entry in the first row of the standard Young tableau represents an up step, while those in the second row represent down steps. The Dyck path corresponding to Fig. 13.7 is given in Fig. 13.8.

In this section we collect some structural results regarding local update moves of FPL models. Following Wieland [78], we define operators G_{ij} that act on the height configurations as follows. They act as the identity on each square except on the square at (i, j) where they either increase or lower the height by 2 if it is allowed. A change of height is allowed if neighbouring heights still differ by one after the change. If it is not allowed, G_{ij} acts as the identity. For future convenience we also

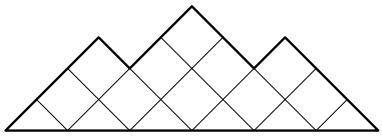

Fig. 13.8 Dyck path corresponding to the FPL diagram in Fig. 13.6 and the standard Young tableau in Fig. 13.7.

define the operators

$$G_0 = \prod_{(i,j)\in S_0} G_{ij}, \quad G_1 = \prod_{(i,j)\in S_1} G_{ij}. \tag{13.2}$$

where G_0 and G_1 denote the even and odd sublattice of the square lattice respectively.

Starting from an initial height configuration, such as the one in Fig. 13.5, the operators G_{ij} generate all height configurations. Put in other words, if we denote the height configuration corresponding to the unit matrix by Z_1, all other allowed height configurations correspond to a word in the operators G_{ij} acting on Z_1.

On a plaquette of an FPL configuration, the involution G acts as

G :  (13.3)

while on other types of plaquettes G acts as the identity. Wieland [78] observed that the operator $G_0 \circ G_1$ "gyrates" a link pattern and that the number of FPL configurations is an invariant under gyration.

We define two other operations on the FPL diagrams, U_{ij} and O_{ij}, that leave the link pattern invariant but that generate all diagrams belonging to a fixed link pattern. The operator U acts on two plaquettes, either horizontally or vertically. Where it acts non-trivially it is given by,

U : 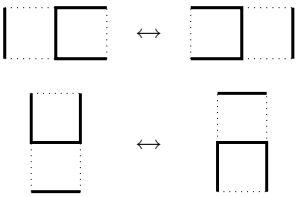 (13.4)

The operator O acts on three plaquettes, either horizontally or vertically. Where it acts non-trivially, it is given by,

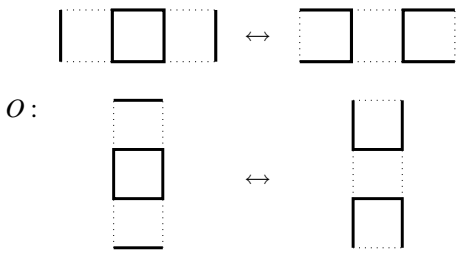

(13.5)

It is easy to see that both U and O leave the link pattern external to the plaquettes on which they act invariant. It is also not difficult to see that on a horizontal strip of arbitrary length, such that only the leftmost and rightmost edge are connected to the outside world, the operators U and O generate all possible FPL diagrams leaving the link pattern invariant. A similar argument holds for vertical strips. This proves that acting with U and O on an FPL diagram with given link pattern, one generates all FPL diagrams corresponding to that link pattern, and no more.

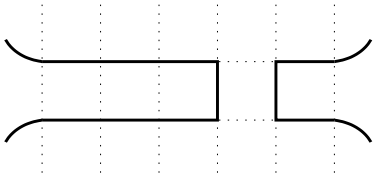

Fig. 13.9 An isolated row inside an FPL configuration: only the leftmost and rightmost edge are connected to the rest of the FPL configuration. The operators U and O generate all possible configurations within the row.

13.2 Partition Function

To each local FPL vertex we assign a weight w_i and define the statistical mechanical partition function Z_n as the sum over all FPL configurations of the product of the vertex weights,

$$Z_n = \sum_{\text{configurations}} \prod_{i=1}^{6} w_i^{k_i}, \tag{13.6}$$

where k_i is the number of vertices of type i. We will consider only the case where the weights on the two sublattices are the same, i.e. in the six-vertex representation the weights are invariant under arrow reversal. Using standard six-vertex notation we write $w_1 = w_2 = a$, $w_3 = w_4 = b$ and $w_5 = w_6 = c$, see Fig. 13.10.

It is convenient to parametrise a, b and c in the following way,

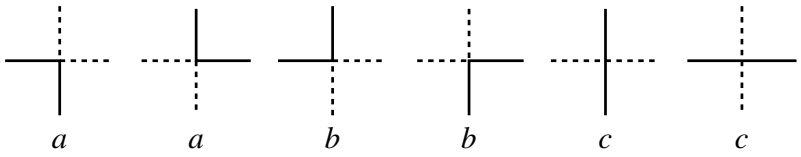

Fig. 13.10 Weights of the six local FPL vertices.

$$a = \sin(\gamma - u), \qquad b = \sin(\gamma + u), \qquad c = \sin(2\gamma), \tag{13.7}$$

and to introduce the u-independent quantity τ by

$$\tau^2 = \frac{c^2 - (a-b)^2}{ab} = 2(1-\Delta) = 4\cos^2\gamma, \tag{13.8}$$

where Δ is the standard notation for the anisotropy parameter of the six-vertex model defined by

$$\Delta = \frac{a^2 + b^2 - c^2}{2ab} = -\cos(2\gamma). \tag{13.9}$$

When $a = b$, $\tau = c/a$ gives a weight to straight loop segments. It is therefore expected that for some critical value of τ there is an ordering transition in the FPL model from a disorder phase to a phase where the vertex with weight c dominates and the polygons are elongated. We will see below that this transition takes place at $\tau = 2$. For $a > b + c$ or $b > a + c$ there is another ordering transition at $\tau = 0$ where the vertices with weight a or b, respectively, dominate.

The partition function Z_n can be computed exactly for finite n applying methods of solvable lattice models to the six-vertex model with domain wall boundary conditions. This was first done by Korepin and Izergin [39, 36, 37] who derived the following determinant expression for Z_n,

$$Z_n = \frac{\left(\sin(\gamma+u)\sin(\gamma-u)\right)^{n^2}}{\left(\prod_{k=0}^{n-1} k!\right)^2}\,\sigma_n, \tag{13.10}$$

where σ_n is the Hankel determinant

$$\sigma_n = \det\left(\frac{\mathrm{d}^{i+k-2}\phi}{\mathrm{d}\,u^{i+k-2}}\right)_{1\le i,k\le n}, \tag{13.11}$$

and

$$\phi(u) = \frac{\sin(2\gamma)}{\sin(\gamma+u)\sin(\gamma-u)}. \tag{13.12}$$

Using the height representation (13.1) it is possible to introduce elliptic weights, rather than the trigonometric weights (13.7). The partition function in that case has been computed by Rosengren [70].

13.2.1 Another Form of the Partition Function

Independent of Izergin and Korepin, in the case $a = b$ (i.e. $u = 0$), another form of Z_n was discovered conjecturally by Robbins in the context of alternating-sign matrices (ASMs) and symmetry classes thereof, see [68]. As can be easily seen from Figures 13.2 and 13.4, a τ weighted FPL configuration, where each straight loop segment is assigned a weight τ, is equal to the generating of weighted ASMs where each nonzero entry is assigned a weight τ. Up to a simple factor, this is also the generating function $A_n(\tau^2)$ of τ^2-weighted ASMs of size $n \times n$ where each -1 is assigned a weight τ^2 (each additional -1 in an ASM also introduces an additional $+1$). The latter was conjectured by Robbins [68] to equal

$$A_{2n}(\tau^2) = 2T_n(\tau^2)R_{n-1}(\tau^2), \qquad A_{2n+1}(\tau^2) = T_n(\tau^2)R_n(\tau^2). \tag{13.13}$$

where

$$T_n(\tau^2) = \det_{1\le i,j\le n}\left(\sum_{r=0}^{2n}\binom{i-1}{r-i}\binom{j}{2j-r}\tau^{2(2j-r)}\right), \tag{13.14}$$

and

$$R_n(\tau^2) = \det_{0\le i,j\le n-1}\left(\sum_{r=0}^{2n-1} Y_{i,r,\mu}Y_{j,r,0}\ \tau^{2(2j+1-r)}\right), \tag{13.15}$$

where

$$Y_{i,r,\mu} = \binom{i+\mu}{2i+1+\mu-r} + \binom{i+1+\mu}{2i+1+\mu-r}. \tag{13.16}$$

The precise correspondence using the notation of the previous section is

$$Z_{2n} = (\sin\gamma)^{2n(2n-1)}\, A_{2n}(4\cos^2\gamma), \tag{13.17a}$$

$$Z_{2n+1} = 2\cos\gamma\,(\sin\gamma)^{2n(2n+1)} A_{2n+1}(4\cos^2\gamma). \tag{13.17b}$$

In fact, Robbins' conjecture was slightly more general and gave a generating function for refined ASMs. The generating functions R and T appear naturally in weighted enumerations of cyclically symmetric plane partitions [53].

The equivalence of the homogeneous limit of Izergin's determinant and Robbins' conjecture, i.e. equation (13.17), is only proved for $\tau = 1$ [81, 42]. Kuperberg and Robbins [43, 68] noticed several other such equivalences between homogeneous Izergin or Tsuchiya[1] type determinants and generating functions of the form (13.14) or (13.15). Some of these were recently proved in [34] using a technique which seems immediately applicable to all the cases considered by Kuperberg and Robbins.

[1] The Tsuchiya determinant is the generating function of horizontally or vertically symmetric FPL diagrams [77]

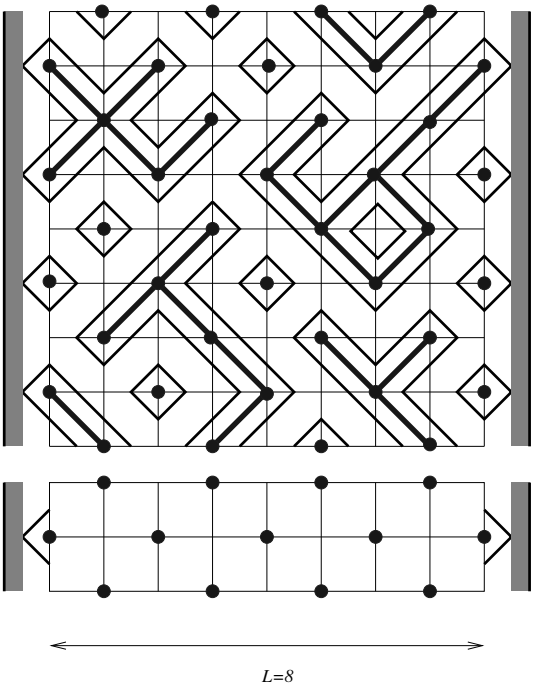

Fig. 13.11 Bond percolation clusters and O(1) cluster boundaries on a semi-infinite strip. Configurations are generated by repeated concatenation of double rows using the double-row transfer matrix. The particular boundary conditions chosen here are called *closed* or *reflecting*.

13.3 Bond Percolation, the O($n = 1$) Model and the Razumov-Stroganov Conjecture

In this section we mention a (partially conjectural) relation between FPL diagrams and the O(1) loop model. We will use this relation to generate FPL statistics in a relatively easy way, without having to explicitly enumerate FPL diagrams.

Imagine that each site of the square lattice is a reservoir of water. With probability p, water percolates between reservoirs along a bond of the square lattice. At $p = 1/2$, the model is critical, and equivalent to the dense O($n = 1$) loop model [12] on a square lattice. The loops of the O(1) model describe the boundaries of the percolation clusters, see Fig. 13.11. Many asymptotic properties such as critical exponents of correlation functions can be computed for the O(n) model using Coulomb gas techniques and conformal field theory, see Chapter 14 for an exhaustive overview. More recently, geometric properties of conformally invariant loops have been analysed using the stochastic Loewner evolution (SLE), see Chapter 15 of this book.

Configurations of the O(1) loop model can be generated using a transfer matrix, see Fig. 13.11 for the particular case of *closed* or *reflecting* boundary conditions. Schematically, the local blocks of the O(1) transfer matrix are given by

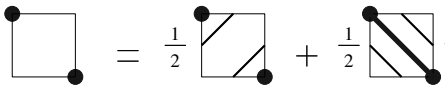

(13.18)

The closed loops of the O(1) loop model have weight $n = 1$. Loops ending on the boundary of the strip define a link pattern. For example, the link pattern corresponding to the bottom side of Fig. 13.11 has link pattern $()()()()$. The transfer matrix T of the O(1) loop model therefore acts on states indexed by a link pattern.

13.3.1 The Razumov-Stroganov Conjecture

The largest eigenvalue of the transfer matrix of the O(1) has eigenvalue 1. It was found in [5, 64, 65, 32, 59] that the corresponding groundstate eigenvector surprisingly is related to the statistics of FPL models. Denoting a link pattern by α and forming a vector space with basis elements $|\alpha\rangle$, the groundstate eigenvector satisfies

$$T|\psi\rangle = |\psi\rangle, \qquad |\Psi\rangle = \sum_{\alpha} \psi_\alpha |\alpha\rangle. \tag{13.19}$$

In the case of periodic boundary conditions, Razumov and Stroganov formulated the following important conjecture:

The coefficient ψ_α equals the number of FPL diagrams with link pattern α.

The RS conjecture generalises to other boundary conditions, in which case the eigenvector coefficient ψ_α of the corresponding transfer matrix enumerates symmetry classes of FPL diagrams, to be discussed below. This is explained in detail in [30]. The case that will be treated in most detail here is the O(1) model on a strip, as in Fig. 13.11, for which ψ_α conjecturally enumerates horizontally symmetric FPL diagrams.

Assuming the RS conjecture, we will use the O(1) loop model to generate FPL statistics by solving (13.19), and variants thereof for other boundary conditions. The particular boundary conditions we will use are *periodic*, *cylindrical* and *closed*. See e.g. [54, 30, 24, 62, 84, 85, 76] for examples and other types of boundary conditions not considered here.

Let us define the norm $\mathcal{N}_L$ of $|\Psi\rangle$ by

$$\mathcal{N}_L = \sum_{\alpha} \psi_\alpha, \tag{13.20}$$

and denote the largest element of $|\Psi\rangle$ by $\psi_{\max}$. The result of solving (13.19) for various boundary conditions is shown in Table 13.1, where the numbers A, A_{HT} and A_{V} are defined by:

- The number of $n \times n$ ASMs,

$$A(n) = \prod_{k=0}^{n-1} \frac{(3k+1)!}{(n+k)!} \;=\; 1,2,7,42,\ldots \tag{13.21}$$

- The number of $n \times n$ half turn symmetric ASMs,

$$\begin{aligned} A_{\mathrm{HT}}(2n) &= A(n)^2 \prod_{k=0}^{n-1} \frac{3k+2}{3k+1} \;=\; 2,10,140,5544,\ldots \\ A_{\mathrm{HT}}(2n-1) &= \prod_{k=1}^{n-1} \frac{4}{3} \left(\frac{(3k)!(k!)}{(2k)!^2} \right)^2 \;=\; 1,3,25,588,\ldots \end{aligned} \tag{13.22}$$

- The number of $(2n-1) \times (2n-1)$ horizontally (or vertically) symmetric ASMs,

$$A_{\mathrm{V}}(2n-1) = \prod_{k=1}^{n-1} (3k-1) \frac{(6k-3)!(2k-1)!}{(4k-2)!(4k-1)!} \;=\; 1,1,3,26,646,\ldots. \tag{13.23}$$

  and its related version for even sizes (also denoted by N_8 in [13]),

$$A_{\mathrm{V}}(2n) = \prod_{k=1}^{n-1} (3k+1) \frac{(6k)!(2k)!}{(4k)!(4k+1)!} \;=\; 1,2,11,170,\ldots \tag{13.24}$$

Table 13.1 The norm and largest eigenvalue of transfer matrices of various types.

Type	$\mathscr{N}_L$	$\psi_{\max}$
Periodic, L even	$A(L/2)$	$A(L/2-1)$
Cylindrical, L even	$A_{\mathrm{HT}}(L)$	$A_{\mathrm{HT}}(L-1)$
Cylindrical, L odd	$A_{\mathrm{HT}}(L)$	$A((L-1)/2)^2$
Closed, L even	$A_{\mathrm{V}}(L+1)$	$A_{\mathrm{V}}(L)$
Closed, L odd	$A_{\mathrm{V}}(L+1)$	$A_{\mathrm{V}}(L)$

Mills et al. conjectured the number of ASMs to be $A(n)$, which was proved more than a decade later by Zeilberger [81] and in an entirely different way by Kuperberg [42]. Kuperberg made essential use of the connection to the six-vertex model and its integrability. Conjectured enumerations of symmetry classes were given by Robbins [68], many of which were subsequently proved by Kuperberg [43]. The properties and history of ASMs are reviewed in the book by Bressoud [13], as well as by Robbins [67] and Propp [61].

13.3.2 Proofs and Other Developments

The sum rules listed in Table 13.1, relating the norms (13.20) of $|\Psi\rangle$ for different boundary conditions to symmetry classes of alternating-sign matrices, were originally obtained conjecturally. These sum rules have been proved algebraically using an inhomogeneous extension of the transfer matrix, a method initiated and developed by Di Francesco and Zinn-Justin [21, 19]. This has led to further interesting directions, not pursued here, such as the connections between weighted FPL diagrams (or ASMs), plane partitions and the q-deformed Knizhnik-Zamolodchikov equation [57, 19, 22, 20, 23, 34].

In an alternative interpretation, the O(1) model is equivalent to a stochastic model defined on link patterns, the so called raise and peel model [33]. It is an open question how to define a stochastic model directly on FPL diagrams, by say the Wieland involutions G describe in Section 13.1.2, such that it has an equipartite stationary state and reduces to the raise and peel model when the action of the operators O and U of Section 13.1.2 is divided out. Such a process would result in a direct proof of the Razumov-Stroganov conjecture.

13.4 Symmetry Classes of FPL Diagrams

We will now focus on FPL models defined on rectangular grids, corresponding to certain symmetry classes of square FPL diagrams. The two main reasons are that for such FPL models there is a natural boundary giving rise to additional structure, and that at the time of writing, for these models more results are known which are relevant to polygon models.

13.4.1 Horizontally Symmetric FPL Diagrams

For horizontally symmetric FPL diagrams (HSFPLs) one only has to consider the lower half of an FPL diagram. As explained in [30], due to geometric constraints one can further reduce the size of such half diagrams. Therefore, for L even, the reduced lower half of a horizontally symmetric FPL diagram of size $(L+1)\times(L+1)$ is an FPL diagram of size $(L-1)\times L/2$. The total number $Z_{\mathrm{HSFPL}}(2n)$ of horizontally (or vertically) symmetric FPL diagrams of size $(2n-1)\times n$ is known, and can be computed from the Tsuchiya determinant [77, 43],

$$Z_{\mathrm{HSFPL}}(2n) = A_{\mathrm{V}}(2n+1) = \prod_{k=1}^{n}(3k-1)\frac{(6k-3)!(2k-1)!}{(4k-2)!(4k-1)!}. \tag{13.25}$$

As can be seen from Table 13.1, this number is equal to the norm $\mathcal{N}_{2n}$ for the O(1) model with closed boundary conditions and $L=2n$. For odd system sizes,

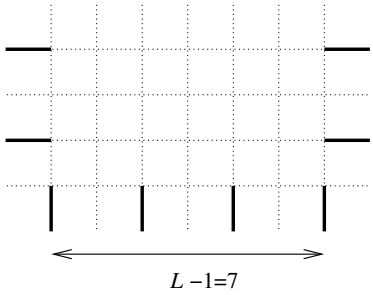

Fig. 13.12 Boundary conditions for an HSFPL diagram of size $(2n-1)\times n = 7\times 4$. The number of external terminals equals $2n = 8$, hence the statistics of this diagram is generated from the O(1) model with $L = 8$.

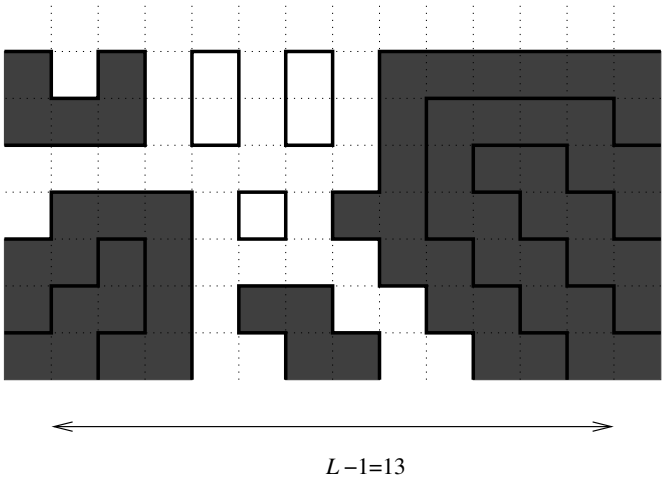

Fig. 13.13 An FPL diagram of size $(L-1)\times L/2 = 13\times 7$ with four nests.

$L = 2n+1$, the norm $\mathscr{N}_L$ equals the number of FPL diagrams of size $L\times(L-1)/2$, which we will denote by $Z_{\mathrm{HSFPL}}(2n+1)$.

There are two interesting and natural statistics on HSFPLs which we will explain now. As noted above, to each FPL diagram is associated a link pattern. Each link pattern factorises in sets of completed links where, in terms of the parenthesis notation, the number of closing parentheses equals the number of opening parentheses. For example,

$$(()())((((())))()() = (()()) \cdot ((((())))) \cdot ().$$

Such completed links are called nests , and they provide a statistic for HSFPLs. An example of an HSFPL diagram of size 13×7 with four nests is given in Fig. 13.13.

Another natural statistic is the number d^* of loops connecting the leftmost loop terminals with the rightmost ones, i.e. loops connecting terminal i with $2\lfloor L/2\rfloor - i+1$ for $i = 1,\ldots,d^*$. It will be convenient to define d by

$$d = \left\lfloor \frac{L-1}{2} \right\rfloor - d^*, \tag{13.26}$$

where d is called the depth of an HSFPL diagram. An example of an HSFPL diagram of size $(L-1) \times L/2 = 13 \times 7$ with three nests and depth $d = 4$ ($d^* = 2$) is given in Fig. 13.14.

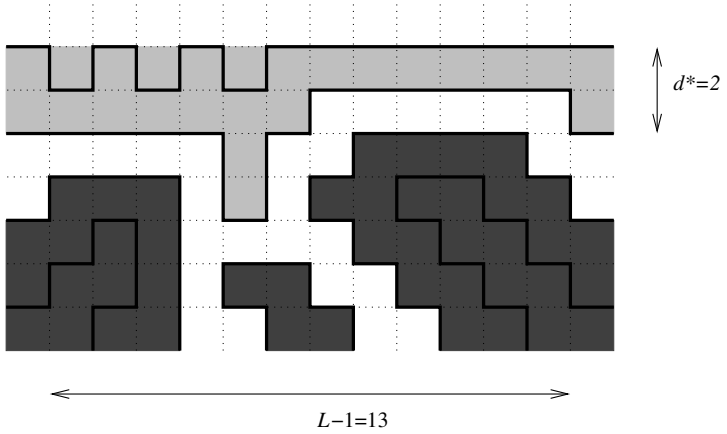

Fig. 13.14 An FPL diagram of size $(L-1) \times L/2 = 13 \times 7$ with three nests and depth $d = 4$ ($d^* = 2$).

13.4.2 Depth-Nest Enumeration of HSFPLs

In this section we will say that an FPL diagram is of size L, if it is of size $(L-1) \times L/2$ if L is even, or of size $L \times (L-1)/2$ if L is odd. Let $P(L,d,m)$ be the number of such FPL diagrams of size L, depth d and having $m+1$ nests. The nest generating function for diagrams of size L and depth d is defined by

$$\mathscr{P}(L,d;z) = \sum_{m=0}^{d} P(L,d,m) z^m. \tag{13.27}$$

Let $S(L,d)$ be the total number of HSFPL diagrams at a given size L and depth d. Obviously we have

$$S(L,d) = \mathscr{P}(L,d;1) = P(L,d+1,0), \tag{13.28}$$

and

$$Z_{\mathrm{HSFPL}}(L) = S(L, \lfloor \tfrac{L-1}{2} \rfloor) = \mathscr{P}(L, \lfloor \tfrac{L-1}{2} \rfloor; 1). \tag{13.29}$$

Based on the RS conjecture, Mitra et al. and Pyatov have conjectured the exact form of $S(L,d)$ [54, 62]. Here we give this conjecture in the following form:

Conjecture 1 The total number of HSFPL diagrams at a given size L and depth d is given by

$$S(L,d)=\prod_{k=0}^{d}\frac{\Gamma(L-k+1)}{2^k(1/2)_k\Gamma(L-2k+1)}\frac{\Gamma(\frac{2L+2k+3}{6})\Gamma(\frac{L-2k+3}{3})}{\Gamma(\frac{2L-k+3}{6})\Gamma(\frac{2L-k+6}{6})}. \tag{13.30}$$

Assuming the RS conjecture, the formula for $S(L,d)$ has recently been proved [34].

Pyatov also found an exact formula for $P(L,d,m)$ [62] which fits exact data for small system sizes ($L\leq 18$). He conjectured that this formula holds for all L, d and m. In terms of the nest generating function this conjecture can be stated as follows.

Conjecture 2 The nest generating function is given by

$$\mathscr{P}(L,d;z)=S(L,d-1)\,{}_3F_2\left(\begin{matrix}-d,L-2d,L-d+\frac{1}{2}\\ -2d,2L-2d+1\end{matrix};4z\right). \tag{13.31}$$

Note that Conjecture 1 follows from Conjecture 2 due to the evaluation

$${}_3F_2\left(\begin{matrix}-d,L-2d,L-d+\frac{1}{2}\\ -2d,2L-2d+1\end{matrix};4\right)=\frac{S(L,d)}{S(L,d-1)}, \tag{13.32}$$

which is a consequence of one of the strange evaluations of Gessel and Stanton [28]. For $d=\lfloor(L-1)/2\rfloor$, the formulas in Conjecture 1 and Conjecture 2 were given in [30].

By convention, $P(L,d,m)$ have the following boundary values:

$$P(L,d,m=-1)=P(L,d,m=-2)=P(L,d,m=d+1)=0\,, \tag{13.33}$$

and we also note the boundary condition

$$P(L,d,m=1)=(L-2d)S(L,d-1)\,. \tag{13.34}$$

It was found in [1] that the function $P(L,d,m)$ is completely determined by these boundary conditions and the following interesting bilinear relation called the *split hexagon relation*,

$$\begin{aligned}&P(L+1,d+1,m)S(L-1,d-1)\\ &\quad=P(L-1,d,m)S(L+1,d)+P(L,d-1,m-2)S(L,d+1).\end{aligned} \tag{13.35}$$

Summing up over $m=0,1,\ldots d+1$ in (13.35) reproduces the hexagon relation, or discrete Boussinesq equation, for $S(L,d)$, see [62].

13.4.2.1 Cyclically Symmetric Transpose Complement Plane Partitions

Somewhat outside the scope of this book, we note the following interesting fact observed in [34]. The total number of nests at a given depth, $S(L,d)$, is equal to the number of punctured cyclically symmetric transpose complement plane partitions [14], see Fig. 13.15. This can be seen by enumerating the number of non-intersecting lattice paths in the South-East fundamental domain of the plane partition. Using the Gessel-Viennot-Lindström method [29, 49] one obtains a determinant of the type (13.14) with $\tau = 1$, which can be evaluated in factorised form [14]. This form equals the expression in (13.30).

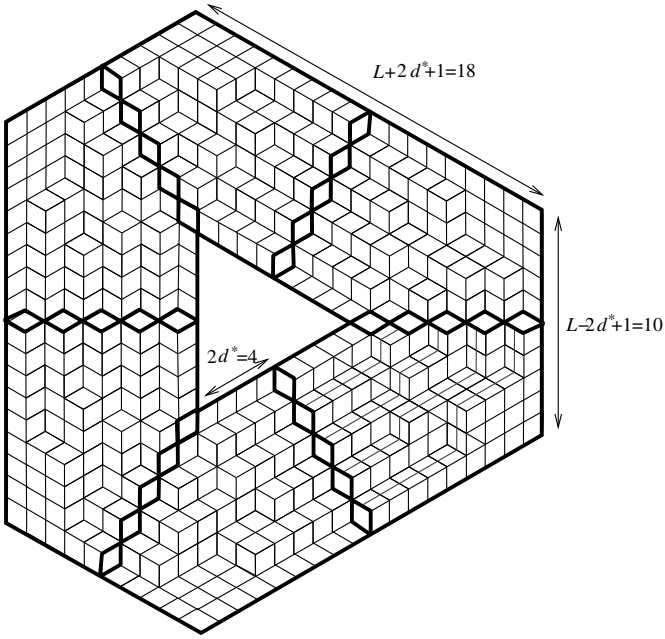

Fig. 13.15 A punctured cyclically symmetric transpose complement plane partition for $L = 13$ and $d^* = 2$.

13.4.3 Average Number of Nests in HSFPL Diagrams

The average number of nests in HSFPL diagrams at depth d and size L, denoted by, $\langle 1 + m \rangle_{d^*}$, is defined as

$$\langle 1+m\rangle_{d^*} = \frac{1}{Z_{\mathrm{HSFPL}}(L)} \sum_{m=0}^{d} (1+m) P(L,d,m)$$
$$\equiv \frac{S(L,d)}{Z_{\mathrm{HSFPL}}(L)} \left(1+\langle m\rangle^{\mathrm{c}}_{d^*}\right). \tag{13.36}$$

For notational clarity we will suppress the dependence of $\langle 1+m\rangle_{d^*}$ on L and recall that

$$d = \left\lfloor \frac{L-1}{2} \right\rfloor - d^*.$$

With the data $P(L,d,m)$ we can calculate $\langle m\rangle^{\mathrm{c}}_{d^*}$:

$$\langle m\rangle^{\mathrm{c}}_{d^*} = \frac{1}{S(L,d)} \sum_{m=1}^{d} m P(L,d,m)$$
$$= \left.\frac{\mathrm{d}}{\mathrm{d}z}\right|_{z=1} \log \mathscr{P}(L,d;z). \tag{13.37}$$

The `Mathematica` implementation of the Gosper-Zeilberger algorithm [35, 79, 80] by Paule and Schorn [58], is able to recognise $\langle m\rangle_{d^*}$ in an almost factorised form. Let $L = 2n$, then define $\mu_n(d^*)$ by

$$\mu_n(d^*) = \sum_{m=0}^{n-1-d^*} \Big(3m + 4(d^*+1)\Big) \frac{P(2n, n-1-d^*, m)}{P(2n, n-1-d^*, 0)}$$
$$= \Big(3\langle m\rangle^{\mathrm{c}}_{d^*} + 4(d^*+1)\Big) \frac{S(2n, n-1-d^*)}{S(2n, n-2-d^*)}. \tag{13.38}$$

The expression $\mu_n(d^*)$ turns out to be summable in factorised form, giving rise to

$$\langle m\rangle^{\mathrm{c}}_{d^*} = -\frac{2}{3}(L-2d) + 2^{2/3} \frac{\Gamma\left(\frac{2L+2d+5}{6}\right)\Gamma\left(\frac{2L-d+3}{3}\right)\Gamma\left(\frac{L-2d+1}{3}\right)}{\Gamma\left(\frac{2L+2d+3}{6}\right)\Gamma\left(\frac{2L-d+2}{3}\right)\Gamma\left(\frac{L-2d}{3}\right)}. \tag{13.39}$$

This formula also holds for odd values of L.

13.4.4 Half-Turn Symmetric FPL Diagrams

In the case of half turn symmetric FPL diagrams (HTSFPLs) it also suffices to consider only the lower half of an FPL diagram, but the boundary conditions on the top row of the half diagram are different from HSFPLs, see Fig. 13.16. The total number of HTSFPL diagrams is given by [43]

$$Z_{\mathrm{HT}}(2n) = A_{\mathrm{HT}}(2n) = 2\prod_{k=1}^{n-1} \frac{3(3k+2)!(3k-1)!k!(k-1)!}{4(2k+1)!^2(2k-1)!^2}. \tag{13.40}$$

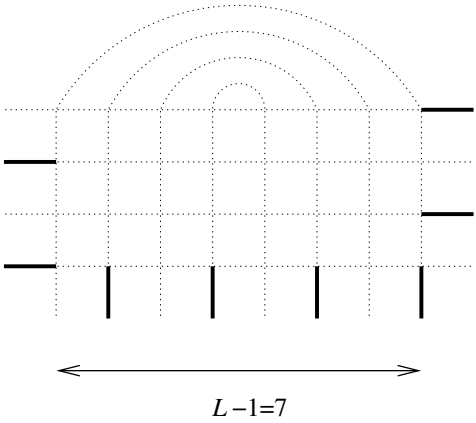

Fig. 13.16 Boundary conditions for an HTSFPL diagram of size $(2n-1)\times n = 7\times 4$. The arcs at the top are additional edges which may contain loop segments. The number of external terminals equals $2n = 8$, hence the statistics of this diagram is generated from the periodic O(1) model with $L = 8$.

Care has to be taken when defining link patterns and nests for HTSFPL diagrams. External terminals can be connected in two distinct ways depending on whether the corresponding loop runs over an odd or even number of the arcs on the top of the diagram. In the case of an odd number of arcs, we exchange the parentheses denoting the connection of a pair of sites. For example, the connectivity of the HTSFPL diagram in Fig. 13.17 is denoted by

$$)\cdot()\cdot()\cdot((),$$

where the dots again denote the factorisation of link pattern into nests. Figure 13.17 thus denotes an HTSFPL diagram with three nests.

As in the case of horizontal symmetry, there exists a conjecture for the nest distribution function [30], but in this case only for $L = 2n$ and $d^* = 0$. Let $P(L,m)$ denote the number of half-turn symmetric FPL diagrams with $m+1$ nests, and define the nest generating function by

$$\mathscr{P}(L;z) = \sum_{m=0}^{n-1} P(L,m)z^m. \tag{13.41}$$

Conjecture 3 The nest generating function for half-turn symmetric FPL diagrams is given by

$$\mathscr{P}(2n;z) = Z_{\mathrm{HTSFPL}}(2n)\frac{3n}{4n^2-1}\,{}_3F_2\left(\begin{matrix}3/2,1-n,1+n\\2-2n,2+2n\end{matrix};4z\right).$$

The average number of nests in HTSFPL diagrams of size $L = 2n$ having $1+m$ nests, denoted by $\langle 1+m\rangle$, is defined as

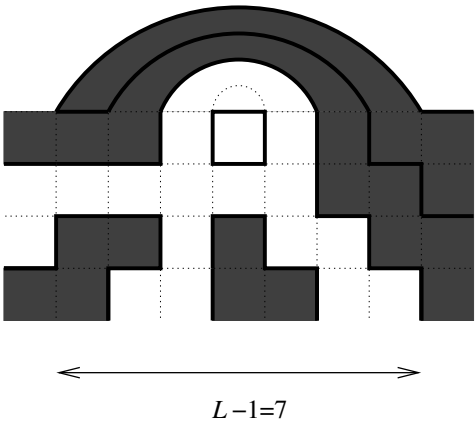

Fig. 13.17 An HTSFPL diagram of size $(2n-1)\times n = 7\times 4$ with link pattern $)\cdot()\cdot()\cdot((),$ having three nests.

$$\langle 1+m\rangle = \frac{1}{Z_{\mathrm{HTSFPL}}(L)}\sum_{m=0}^{n-1}(1+m)P(L,d,m) = 1+z\frac{\mathrm{d}}{\mathrm{d}z}\log\mathscr{P}(L;z) \qquad (13.42)$$

Knowing the nest generating function we may compute $\langle 1+m\rangle$, which turns out to be summable [30].

Conjecture 4 The average number of nests in HTSFPL diagrams of size L, is given by

$$\langle 1+m\rangle = n\prod_{j=1}^{n-1}\frac{3j+1}{3j+2}.$$

13.5 Phase Transitions

13.5.1 Bulk Asymptotics and Phase Diagram

The phase diagram of the FPL model can be derived from the asymptotics of the partition function Z_n defined in (13.10). The leading asymptotics of Z_n for general values of τ has been computed by Korepin and Zinn-Justin [41] using the Toda equation satisfied by σ_n [74],

$$\sigma_n\frac{\mathrm{d}^2\sigma_n}{\mathrm{d}u^2} - \left(\frac{\mathrm{d}\sigma_n}{\mathrm{d}u}\right)^2 = \sigma_{n+1}\sigma_{n-1}. \qquad (13.43)$$

Writing σ_n as a matrix model integral [83], further subleading asymptotics were computed by Bleher and Fokin [10] and Bleher and Liechty [11] using orthogonal

polynomials. For special values of γ this method was first employed by Colomo and Pronko [17]. The final result for $0 < \tau^2 = 4\cos^2\gamma < 4$ $(1 > \Delta > -1)$ is that for some $\varepsilon > 0$,

$$Z_n = Cn^{\kappa} \exp\left[fn^2(1 + \mathcal{O}(n^{-\varepsilon}))\right], \tag{13.44}$$

where C is a constant and

$$f = \frac{\pi \, \sin(\gamma+u)\sin(\gamma-u)}{2\gamma\cos(\pi u/2\gamma)}, \tag{13.45}$$

$$\kappa = \frac{1}{12} - \frac{2\gamma^2}{3\pi(\pi-2\gamma)}. \tag{13.46}$$

The result (13.44) is valid in the so-called disordered (D) phase $0 < \tau^2 < 4$. There is a phase transition to an ordered phase at $\tau^2 = 4$ where the vertices with weight c are favoured and the perimeters of the polygons in the FPL model consist of elongated straight lines. In terms of the six-vertex model this is called the anti-ferromagnetic (AF) phase. At $\tau = 0$, i.e. $a = b + c$ or $b = a + c$, there is another phase transition to a so-called ferromagnetic phase, where, respectively, the a- or b-type vertices dominate. The complete phase diagram is given in Fig. 13.18.

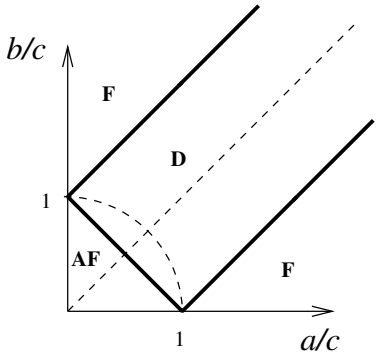

Fig. 13.18 Bulk phase diagram of the FPL model. The phases are traditionally called disordered (D), ferro-electric (F) and anti-ferro-electric (AF), cf. the six-vertex model. The arc corresponds to the free-fermion condition $\Delta = 0$ $(\tau^2 = 2)$, and the line $a = b$ corresponds to τ^2-enumerations of ASMs. On this line $\tau^2 = c^2/a^2 = 2(1-\Delta)$, and the D-AF phase transition takes place at $\tau^2 = 4$.

The phase diagram and the Bethe-Ansatz solution of the six-vertex model for *periodic* and *anti-periodic* boundary conditions are thoroughly discussed in the works of Lieb [45, 46, 47], Lieb and Wu [48], Sutherland [73], Baxter [7], and Batchelor et al. [3].

13.5.2 Asymptotics for Symmetry Classes at $\tau = 1$

In this section we determine the asymptotics of equally weighted horizontally and half-turn symmetric FPL diagrams for $\tau = 1$ or $\gamma = 2\pi/3$, corresponding to the numbers given in Table 13.1. The leading asymptotic form of these numbers, which are all products over factorials, can be computed using the Euler-Maclaurin approximation. Full asymptotics can easily be derived using Barnes' G-function [2], which satisfies

$$G(z+1) = \Gamma(z)G(z), \qquad G(1) = 1, \tag{13.47}$$

and whose leading asymptotic behaviour is given by (see e.g. [56]),

$$\log(G(z+1)) = z^2\left(\frac{1}{2}\log z - \frac{3}{4}\right) + \frac{1}{2}z\log 2\pi - \frac{1}{12}\log z + \mathscr{O}(1). \tag{13.48}$$

In the case of $A(n)$ and $A_{\mathrm{HT}}(n)$, a detailed asymptotic analysis including the lower order terms was carried out by Mitra and Nienhuis [55]. Here we list only the leading asymptotics of the FPL numbers relevant to the current context. The generic asymptotic form of the numbers is

$$\log Z_L = s_0\ \text{Area} + f_0\ \text{Surface} + x\log(\text{Length}) + \mathscr{O}(1), \tag{13.49}$$

where the bulk and boundary entropies are given by

$$s_0 = \log\left(\frac{3\sqrt{3}}{4}\right), \qquad f_0 = \log\left(\frac{3\sqrt{3}}{4\sqrt{2}}\right). \tag{13.50}$$

The critical exponent x is a universal quantity. In detail, the cases relevant for this chapter are

- FPL diagrams, L even
  The number $A(L/2)$ counts FPL configurations on an $L/2 \times L/2$ square grid, the area of which is $\frac{1}{4}L^2$. We thus find,

$$\log Z(L) = \log A(L/2) = \frac{1}{4}s_0L^2 - \frac{5}{36}\log L + O(1). \tag{13.51}$$

- Half turn symmetric FPL diagrams, L even
  $A_{\mathrm{HT}}(L)$ counts the number of FPL configurations on half an $L \times L$ square grid, the area of which is $\frac{1}{2}L^2$. We thus find for L even,

$$\log Z_{\mathrm{HT}}(L) = \log A_{\mathrm{HT}}(L) = \frac{1}{2}s_0L^2 + \frac{1}{18}\log L + O(1). \tag{13.52}$$

- Half turn symmetric FPL diagrams, L odd
  $A_{\mathrm{HT}}(L)$ counts the number of FPL configurations on a square grid of dimension $L \times (L-1)/2$, the area of which is $\frac{1}{2}L(L-1)$. We thus find for L odd,

$$\log Z_{\mathrm{HT}}(L) = \log A_{\mathrm{HT}}(L) = \frac{1}{2} s_0 L(L-1) + \frac{1}{36}\log L^2 + O(1). \tag{13.53}$$

- Horizontally symmetric FPL diagrams, L even
  $A_{\mathrm{V}}(L+1)$ counts the number of FPL configurations on an $(L-1)\times L/2$ rectangular grid. We find,

$$\log Z_{\mathrm{HSFPL}}(L) = \log A_{\mathrm{V}}(L+1) = \frac{1}{2} s_0 L(L-1) + f_0 L - \frac{5}{72}\log L + O(1). \tag{13.54}$$

- Horizontally symmetric FPL diagrams, L odd
  For L odd, $A_{\mathrm{V}}(L+1)$ counts the number of FPL configurations on a $L\times(L-1)/2$ rectangular grid. We find,

$$\log Z_{\mathrm{HSFPL}}(L) = \log A_{\mathrm{V}}(L+1) = \frac{1}{2} s_0 L(L-1) + f_0 L + \frac{7}{72}\log L + O(1). \tag{13.55}$$

Note that because the upper boundary for FPL diagrams corresponding to HSFPLs is not fixed, see e.g. Fig. 13.12, there is a nonzero boundary entropy in $\log Z_{\mathrm{HSFPL}}(L)$.

13.5.3 Nest Phase Transitions

From Section 13.4.3 we recall that the average number of nests is given by $\frac{S(L,d)}{Z_{\mathrm{HSFPL}}(L)}(1+\langle m\rangle^{\mathrm{c}}_{d^*})$ where

$$\langle m\rangle^{\mathrm{c}}_{d^*} = z\frac{\mathrm{d}}{\mathrm{d}z}\log \mathscr{P}(L,d;z), \tag{13.56}$$

with $\mathscr{P}(L,d;z)$ given in Conjecture 2. The asymptotics for $\langle m\rangle^{\mathrm{c}}_{d^*}$ as $L\to\infty$ can be derived from the hypergeometric equation satisfied by $\mathscr{P}(L,d;z)$. Taking $L=2n$ this gives

$$\begin{aligned}\theta(\theta+1+2d^*-2n)(\theta+2+2d^*+2n)\mathscr{P}(2n,d;z) = \\ 4z(\theta+2+d^*)(\theta+1+d^*-n)(\theta+3/2+n)\mathscr{P}(2n,d;z),\end{aligned} \tag{13.57}$$

where $\theta = z\,\mathrm{d}/\mathrm{d}z$ and

$$d = \left\lfloor \frac{L-1}{2} \right\rfloor - d^* = n-1-d^*. \tag{13.58}$$

Assuming that $d^* = \mathscr{O}(1)$, we discriminate the cases $z<1$, $z=1$ and $z>1$.

- $z<1$
  In this case, up to an overall constant factor, the leading asymptotics of $\mathscr{P}(2n,d;z)$ will be polynomial in n. Neglecting lower order terms, equation (13.57) reduces to,

$$\theta\,\mathscr{P}(2n,d;z) = z(\theta+2+d^*)\mathscr{P}(2n,d;z). \tag{13.59}$$

We thus we find $(1-z)\mathscr{P}'(2n,d;z) = (2+d^*)\mathscr{P}(2n,d;z)$ and

$$\langle m\rangle^{\mathrm{c}}_{d^*} = (2+d^*)\frac{z}{1-z} \qquad (n\to\infty). \tag{13.60}$$

- $z=1$
  In (13.39) an exact expression was given for $\langle m\rangle^{\mathrm{c}}_{d^*}$ at $z=1$. Asymptotically we find that for $L-2d=\mathscr{O}(1)$,

$$\langle m\rangle^{\mathrm{c}}_{d^*} \approx \frac{\Gamma(\frac{L-2d+1}{3})}{\Gamma(\frac{L-2d}{3})} L^{2/3} + \mathscr{O}(1), \tag{13.61}$$

  which for $L=2n$ can be written as

$$\langle m\rangle^{\mathrm{c}}_{d^*} \approx \frac{\Gamma(\frac{2d^*+3}{3})}{\Gamma(\frac{2d^*+2}{3})} (2n)^{2/3} + \mathscr{O}(1), \tag{13.62}$$

- $z>1$
  In this case, and when d is of order n, the leading asymptotics of $\mathscr{P}(2n,d;z)$ will be of the form $p(n)z^n$, where $p(n)$ is a polynomial in n. This means that $\theta\mathscr{P}(2n,d;z)$ is of the same order as $n\mathscr{P}(2n,d;z)$ and (13.57) reduces in leading order to

$$(\theta^3 - 4n^2\theta)\mathscr{P}(2n,d;z) = 4z(\theta^3 - n^2\theta)\mathscr{P}(2n,d;z). \tag{13.63}$$

  Using (13.56) one can derive the following equation for $\langle m\rangle^{\mathrm{c}}_{d^*}$,

$$4n^2(z-1)\langle m\rangle^{\mathrm{c}}_{d^*} = (4z-1)\left(\theta^2\langle m\rangle_{d^*} + 3\langle m\rangle^{\mathrm{c}}_{d^*}\theta\langle m\rangle^{\mathrm{c}}_{d^*} + (\langle m\rangle^{\mathrm{c}}_{d^*})^3\right), \tag{13.64}$$

  which in leading order when $\langle m\rangle^{\mathrm{c}}_{d^*}\sim n$ reduces to $(4z-1)(\langle m\rangle^{\mathrm{c}}_{d^*})^2 = 4n^2(z-1)$ and thus

$$\langle m\rangle^{\mathrm{c}}_{d^*} \approx \sqrt{\frac{z-1}{4z-1}}\, L + \mathscr{O}(1). \tag{13.65}$$

The scaling behaviour near the phase transition at $z=1$ is governed by a single exponent, the cross-over exponent ϕ [9]. On general grounds one expects,

$$\langle m\rangle^{\mathrm{c}}_{d^*} \sim \begin{cases} L(z-1)^{1/\phi-1} & (z>1) \\ L^{\phi} & (z=1) \\ (1-z)^{-1} & (z<1) \end{cases}. \tag{13.66}$$

Indeed, we find such scaling behaviour for $\langle m\rangle^{\mathrm{c}}_{d^*}$ with $\phi = 2/3$.

13.5.3.1 Scaling Function

In [33] an analysis has been carried out to obtain the nest scaling function for $L=2n$ and $d=n-1$, i.e. $d^*=0$. Following Polyakov [60], we expect the following scaling form of the nest distribution function at the critical point,

$$\frac{P(2n,n-1,m)}{S(2n,n-1)} \sim \frac{1}{\langle 1+m\rangle_0} f\left(\frac{1+m}{\langle 1+m\rangle_0}\right) \qquad (n\to\infty), \tag{13.67}$$

where $\langle 1+m\rangle_0 = 1+\langle m\rangle_0^{\mathrm{c}}$. The large x behaviour of $f(x)$ is related to the exponent ϕ [15],

$$\lim_{x\to\infty} f(x) \sim x^s \,\mathrm{e}^{-ax^\delta}, \qquad \delta = \frac{1}{1-\phi}, \tag{13.68}$$

where a and s are constants. The behaviour of $f(x)$ for small x is related to the large n behaviour of the probability $P(2n,n-1,m)/S(2n,n-1)$,

$$\lim_{x\to 0} f(x) = bx^\vartheta \quad \Rightarrow \quad b = \lim_{m\to 0}\lim_{n\to\infty} (1+\langle m\rangle_0)^{1+\vartheta}\, \frac{P(2n,n-1,m)}{S(2n,n-1)}, \tag{13.69}$$

from which we find

$$\vartheta = 1, \qquad b = \frac{3}{\Gamma(2/3)^3}. \tag{13.70}$$

Assuming that the *full* scaling function is of the form $x^\vartheta \,\mathrm{e}^{-ax^\delta}$, for all values of x, and using the normalisation condition

$$\int_0^\infty f(x)\,\mathrm{d}x = 1, \tag{13.71}$$

we find that

$$f(x) = bx\,\mathrm{e}^{-bx^3/3}. \tag{13.72}$$

In Fig. 13.19 we compare the scaling function (13.72) with a numerical evaluation of (13.67) for $n=300$. When $\delta^*>0$, the value of ϕ, and hence that of δ, is not changed, but it follows from (13.69) that the value of the exponent ϑ changes to

$$\vartheta = 1+2d^*. \tag{13.73}$$

The full scaling function is not known in this case.

13.5.4 Half Turn Symmetry

The following analysis closely follows that of the previous section. We are interested in the asymptotics as $n\to\infty$ of the average number of nests defined in (13.56). This can be inferred from the hypergeometric equation for $\mathscr{P}(2n;z)$,

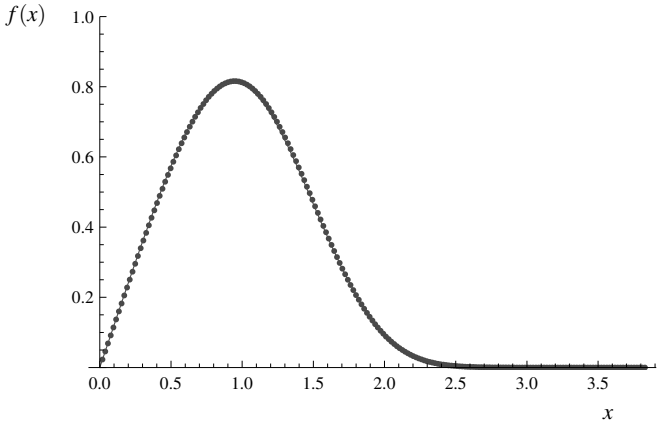

Fig. 13.19 The scaling function $f(x)$ defined in (13.72) compared to a numerical evaluation (dots) of (13.67) for $L = 2n = 600$. It can be seen that these are indistinguishable.

$$\theta(\theta+1+2n)(\theta+1-2n)\mathscr{P}(2n;z) = 4z(\theta+3/2)(\theta+1-n)(\theta+1+n)\mathscr{P}(2n;z). \tag{13.74}$$

Again we discriminate the cases $z<1$, $z=1$ and $z>1$ and remind the reader that $L=2n$.

- $z<1$
  In this case, up to an overall constant prefactor, $\mathscr{P}(2n;z)$ will grow as a polynomial in n and, neglecting lower order terms, (13.74) reduces to,

  $$\theta\mathscr{P}(2n;z) = z(\theta+3/2)\mathscr{P}(2n;z), \tag{13.75}$$

  so that we find $(1-z)\mathscr{P}'(2n;z) = \frac{3}{2}\mathscr{P}(2n;z)$ and thus

  $$\langle 1+m\rangle \approx \frac{2+z}{2(1-z)} + \mathscr{O}(1). \tag{13.76}$$

- $z=1$
  For this case, and exact expression was given for $\langle m+1\rangle$ in Conjecture 4. Asymptotically we find

  $$\langle 1+m\rangle = n\prod_{j=1}^{n-1}\frac{3j+1}{3j+2} \approx \frac{\Gamma(5/6)}{\sqrt{\pi}}\,L^{2/3} + \mathscr{O}(1). \tag{13.77}$$

- $z>1$
  Here,up to an overall constant prefactor, $\mathscr{P}(2n;z)$ will grow as $p(n)z^n$ where $p(n)$ is a polynomial in n. This means that $\theta\mathscr{P}(2n;z)$ will be of the same order as $n\mathscr{P}(2n;z)$ and (13.74) reduces in leading order to

$$(\theta^3 - 4n^2\theta)\mathscr{P}(2n;z) = 4z(\theta^3 - n^2\theta)\mathscr{P}(2n;z), \tag{13.78}$$

which is the same as (13.63). We thus find that

$$\langle 1+m\rangle \approx \sqrt{\frac{z-1}{4z-1}}\,L + \mathscr{O}(1). \tag{13.79}$$

For half-turn symmetric FPL diagrams we find the same cross-over exponent $\phi = 2/3$ as for horizontally symmetric FPL diagrams.

13.6 Conclusion

We have described a model of tightly packed, nested polygons on the square lattice. We hope that the study of such tightly packed polygons is relevant to other polygon models described in this book. The advantage of the model described in this chapter is that many exact results can be obtained, even on finite geometries, due to its relation with the exactly solvable six-vertex and O($n = 1$) lattice models. In particular, the statistical mechanical partition function can be obtained rigorously on finite square patches of the square lattice. The free energy can then be obtained analytically and in the thermodynamic limit. The fully packed loop model undergoes a well-known bulk order–disorder phase transition as a function of an anisotropy parameter associated to the straight segments of the polygon boundary.

We have furthermore shown that it is possible to obtain closed-form expressions for partition functions of important subsets of fully packed loop configurations. Two examples of such subsets are horizontally symmetric fully packed loop models of depth d, and half-turn symmetric fully packed loop models of depth d. These closed-form expressions have been obtained experimentally, and remain conjectures at the time of this writing. In addition, using hypergeometric summation identities, we were able to compute the average number of polygon nests at the boundary in closed form. Asymptotic analyses allowed us to study a boundary phase transition as a function of the nest fugacity, and we obtained a crossover exponent $\phi = 2/3$. At criticality, we derive a scaling form for the nest distribution function which displays an unusual non-Gaussian cubic exponential behaviour.

To conclude, it should be said that while some of the exact results presented in this chapter are more than what one would hope for from a physicist's perspective, where numerical techniques are often all what is available, they are just the starting point for a mathematician. Although great progress has been made in recent years in understanding fully packed loop models, proving conjectures such as the nest distribution function and many related combinatorial results, remains a fascinating and completely open problem. It is for reasons such as these that polygon models in all shapes and sizes will continue to inspire future research.

References

1. F.C. Alcaraz, P. Pyatov and V. Rittenberg, *Density profiles in the raise and peel model with and without a wall. Physics and combinatorics*, J. Stat. Mech. (2008), P01006; arXiv:0709.4575.
2. E. W. Barnes, *Genesis of the double gamma function*, Proc. London Math. Soc. **31** (1899), 358–381; *The theory of the G-function*, Quart. J. Math. **31** (1900), 264–314; *The theory of the double gamma function*, Philos. Trans. R. Soc. London Ser. A **196** (1901), 265–388.
3. M. T. Batchelor, R. J. Baxter, M. J. O'Rourke and C. M. Yung, *Exact solution and interfacial tension of the six-vertex model with anti-periodic boundary conditions*, J. Phys. A **28** (1995), 2759–2770.
4. M. T. Batchelor, H. W. J. Blöte, B. Nienhuis and C. M. Yung, *Critical behaviour of the fully packed loop model on the square lattice*, J. Phys. A, 29 (1996), L399–L404.
5. M. T. Batchelor, J. de Gier and B. Nienhuis, *The quantum symmetric XXZ chain at* $\Delta = -\frac{1}{2}$*, alternating-sign matrices and plane partitions*, J. Phys. A, 34 (2001), L265–L270; arXiv:cond-mat/0101385.
6. M. T. Batchelor, J. de Gier and B. Nienhuis, *The rotor model and combinatorics*, Int. J. Mod. Phys. B, 16 (2002), 1883–1889.
7. R. J. Baxter, *Exactly solved models in statistical mechanics*, Academic Press, San Diego (1982).
8. R. J. Baxter, *Solving models in statistical mechanics*, Adv. Stud. Pure Math., 19 (1989), 95–116.
9. K. Binder, in *Phase Transitions and Critical Phenomena* **8**, eds. C. Domb and J.L. Lebowitz, Academic Press Inc., London (1983), 2.
10. P.M. Bleher and V.V. Fokin, *Exact Solution of the Six-Vertex Model with Domain Wall Boundary Conditions. Disordered Phase*, Commun. Math. Phys. **268** (2006), 223–284; arXiv:math-ph/0510033.
11. P.M. Bleher and K. Liechty, *Exact Solution of the Six-Vertex Model with Domain Wall Boundary Conditions. Ferroelectric phase*, arXiv:0712.4091.
12. H. W. J. Blöte and B. Nienhuis, *Critical behaviour and conformal anomaly of the O(n) model on the square lattice*, J. Phys. A **9** (1989), 1415–1438.
13. D. M. Bressoud, *Proofs and Confirmations: The story of the Alternating Sign Matrix Conjecture*, Cambrige University Press, Cambridge (1999).
14. M. Ciucu and C. Krattenthaler, *Plane partitions II:* $5\frac{1}{2}$ *symmetry classes*, in: Combinatorial Methods in Representation Theory, M. Kashiwara, K. Koike, S. Okada, I. Terada, H. Yamada, eds., Advanced Studies in Pure Mathematics, vol. **28**, RIMS, Kyoto, 2000, 83–103; arXiv:math/9808018.
15. J. des Cloizeaux and G. Jannink, *Polymers in Solution*, Clarendon Press, Oxford (1990).
16. M. Ciucu and C. Krattenthaler, *Enumeration of lozenge tilings of hexagons with cut off corners*, J. Combin. Theory Ser. A **100** (2002), 201–231.
17. F. Colomo and A.G. Pronko, *Square ice, alternating sign matrices, and classical orthogonal polynomials*, J.Stat.Mech. 0501 (2005), P005; arXiv:math-ph/0411076.
18. D. Dei Cont and B. Nienhuis, *The packing of two species of polygons on the square lattice*; J. Phys. A **37** (2004), 3085–3100; arXiv:cond-mat/0311244.
19. P. Di Francesco, *Boundary qKZ equation and generalized Razumov–Stroganov sum rules for open IRF models*, J. Stat. Mech. (2005), P11003; arXiv:math-ph/0509011.
20. P. Di Francesco, *Open boundary Quantum Knizhnik–Zamolodchikov equation and the weighted enumeration of symmetric plane partitions*, J. Stat. Mech. (2007), P01024; arXiv:math-ph/0611012.
21. P. Di Francesco and P. Zinn-Justin, *Around the Razumov-Stroganov conjecture: proof of a multi-parameter sum rule*, 2005 Electron. J. Combin. **12**, R6; arXiv:math-ph/0410061.
22. P. Di Francesco and P. Zinn-Justin, *Quantum Knizhnik-Zamolodchikov equation, generalized Razumov–Stroganov sum rules and extended Joseph polynomials*, J. Phys. A **38** (2005), L815–L822; arXiv:math-ph/0508059.

23. P. Di Francesco and P. Zinn-Justin, *Quantum Knizhnik–Zamolodchikov equation: reflecting boundary conditions and combinatorics*, J. Stat. Mech. (2007), P12009,; arXiv:0709.3410.
24. Ph. Duchon, *On the link pattern distribution of quarter-turn symmetric FPL configurations*, arXiv:0711.2871.
25. N. Elkies, G. Kuperberg, M. Larsen, and J. Propp, *Alternating-Sign Matrices and Domino Tilings*, J. Algebraic Combin., 1 (1992), pp. 111–132 and 219–234.
26. V. Fridkin, Yu. G. Stroganov and D. Zagier, *Groundstate of the quantum symmetric finite-size XXZ spin chain with anisotropy parameter* $\Delta = \frac{1}{2}$, J. Phys. A **33** (2000), L121–L125; arXiv:hep-th/9912252
27. V. Fridkin, Yu. G. Stroganov and D. Zagier, *Finite-size XXZ spin chain with anisotropy parameter* $\Delta = \frac{1}{2}$, J. Stat. Phys. **102** (2001), 781–794; arXiv:nlin.SI/0010021.
28. I. Gessel and D. Stanton, *Strange evaluations of hypergeometric series*, SIAM J. Math. Anal. **13** (1982), 295–308.
29. I. Gessel and X. Viennot, *Binomial determinants, paths, and hook length formulae*, Adv. Math. **58** (1985), 300–321.
30. J. de Gier, *Loops, matchings and alternating-sign matrices*, Discr. Math. **298** (2005), 365–388, arXiv:math.CO/0211285.
31. J. de Gier, M.T. Batchelor, B. Nienhuis and S. Mitra, *The XXZ chain at* $\Delta = -1/2$*: Bethe roots, symmetric functions and determinants*, J. Math. Phys. **43** (2002), 4135–4146; texttarXiv:math-ph/0110011
32. J. de Gier, B. Nienhuis, P. A. Pearce and V. Rittenberg, *A new universality class for dynamical processes*, Phys. Rev. E **67** (2002), 016101–016104; arXiv:cond-mat/0205467, arXiv:cond-mat/0108051.
33. J. de Gier, B. Nienhuis, P. A. Pearce and V. Rittenberg, *The raise and peel model of a fluctuating interface*, J. Stat. Phys. **114** (2004), 1–35; arXiv:cond-mat/0301430
34. J. de Gier, P. Pyatov and P. Zinn-Justin, *Punctured plane partitions and the q-deformed Knizhnik-Zamolodchikov and Hirota equations*, arXiv:0712.3584.
35. R.W. Gosper, *Decision procedure for indefinite hypergeometric summation*, Proc. Natl. Acad. Sci. USA **75** (1978), 40–42.
36. A. G. Izergin, *Partition function of the six-vertex model in a finite volume*, Dokl. Akad. Nauk SSSR **297** (1987), 331–333 (Sov. Phys. Dokl. **32** (1987), 878–879).
37. A. G. Izergin, D. A. Coker and V. E. Korepin, *Determinant formula for the six-vertex model*, J. Phys. A **25** (1992), 4315–4334.
38. N. Kitanine, J. M. Maillet, N. A. Slavnov and V. Terras, *Emptiness formation probability of the XXZ spin-1/2 Heisenberg chain at* $\Delta = 1/2$, J. Phys. A **35** (2002), L385–L388; arXiv:hep-th/0201134.
39. V. E. Korepin, *Calculation of norms of Bethe wave functions*, Commun. Math. Phys. **86** (1982), 391–418.
40. V. E. Korepin, N. M. Bogoliubov and A. G. Izergin, *Quantum inverse scattering method and correlation functions*, Cambridge University Press, Cambridge (1993).
41. V. Korepin and P. Zinn-Justin, *Thermodynamic limit of the six-vertexmodel with domain wall boundary conditions*, J. Phys. A **33** (2000), 7053–7066; arXiv:cond-mat/0004250.
42. G. Kuperberg, *Another proof of the alternating sign matrix conjecture*, Invent. Math. Res. Notes, (1996), 139–150; arXiv:math.CO/9712207.
43. G. Kuperberg, *Symmetry classes of alternating-sign matrices under one roof*, Ann. Math. **156** (2002), 835–866; arXiv:math.CO/0008184.
44. D. Levy, *Algebraic structure of translation invariant spin-*$1/2$ *XXZ and q-Potts quantum chains*, Phys. Rev. Lett. **67** (1991), 1971-1974.
45. E.H. Lieb, *Exact solution of the problem of the entropy of two-dimensional ice*, Phys. Rev. Lett. **18** (1967), 692.
46. E.H. Lieb, *Exact solution of the two-dimensional Slater KDP model of an antiferroelectric*, Phys. Rev. Lett. **18** (1967), 1046–1048.
47. E. H. Lieb, *Exact solution of the two-dimensional Slater KDP model of a ferroelectric*, Phys. Rev. Lett. **19** (1967), 108–110.

48. E. H. Lieb and F. Y. Wu, *Two dimensional ferroelectric models*, in Phase transitions and critical phenomena **1** (Academic Press, 1972), C. Domb and M. Green eds., 331–490.
49. B. Lindström, *On the vector representations of induced matroids*, Bull. London Math. Soc. **5** (1973), 85–90.
50. P. P. Martin *Potts models and related problems in statistical mechanics*, World Scientific, Singapore (1991).
51. W. H. Mills, D. P. Robbins and H. Rumsey, *Proof of the MacDonald conjecture*, Invent. Math., 66 (1982), 73–87.
52. W. H. Mills, D. P. Robbins and H. Rumsey, *Alternating-sign matrices and descending plane partitions*, J. Combin. Theory Ser. A **34** (1983), 340–359.
53. W. H. Mills, D. P. Robbins and H. Rumsey, *Enumeration of a symmetry class of plane partitions*, Discr. Math. **67** (1987), 43–55.
54. S. Mitra, B. Nienhuis, J. de Gier and M. T. Batchelor, JSTAT (2004), P09010; `arXiv:cond-mat/0401245`.
55. S. Mitra and B. Nienhuis, *Exact conjectured expressions for correlations in the dense O(1) loop model on cylinders*, JSTAT (2004), P10006; `arXiv:cond-mat/0407578`.
56. S. Mitra, *Exact asymptotics of the characteristic polynomial of the symmetric Pascal matrix*, J. Combin. Theory Ser. A, in press; `arXiv:0708.1763`
57. V. Pasquier, *Quantum incrompressibility and Razumov Stroganov type conjectures*, Ann. Henri Poincare' **7** (2006) 397–421; `arXiv:cond-mat/0506075`.
58. P. Paule and M. Schorn, *A Mathematica version of Zeilberger's algorithm for proving binomial coefficient identities*, J. Symb. Comp. **20** (1995), 673–698.
59. P. A. Pearce, V. Rittenberg, J. de Gier and B. Nienhuis, *Temperley-Lieb stochastic processes* J. Phys. A **35** (2002), L661–L668; `arXiv:math-ph/0209017`.
60. V. Polyakov, *Zh. Eksp. Theor. Fiz.* **59** (1970), 542.
61. J. Propp, *The many faces of the alternating-sign matrices*, Discrete Mathematics and Theoretical Computer Science Proceedings AA (2001), 43–58.
62. P. Pyatov, *Raise and Peel Models of fluctuating interfaces and combinatorics of Pascal's hexagon*, J. Stat. Mech. (2004), P09003; `arXiv:math-ph/0406025`.
63. A. V. Razumov and Yu. G. Stroganov *Spin chains and combinatorics*, J. Phys. A **34** (2001), 3185–3190; `arXiv:cond-mat/0012141`.
64. A. V. Razumov and Yu. G. Stroganov, *Combinatorial nature of ground state vector of O(1) loop model*, Theor. Math. Phys. **138** (2004), 333–337; Teor. Mat. Fiz. **138** (2004), 395–400; `arXiv:math.CO/0104216`.
65. A. V. Razumov and Yu. G. Stroganov, *O(1) loop model with different boundary conditions and symmetry classes of alternating-sign matrices*, Theor. Math. Phys. **142** (2005) 237–243; Teor. Mat. Fiz. **142** (2005), 284–292; `arXiv:math.CO/0108103`.
66. A. V. Razumov and Yu. G. Stroganov, *Spin chains and combinatorics: twisted boundary conditions*, J. Phys. A **34** (2001), 5335–5340; `arXiv:cond-mat/0102247`.
67. D.P. Robbins, *The story of* $1, 2, 7, 42, 429, 7436, \ldots$, Math. Intelligencer **13** (1991), 12–19.
68. D.P. Robbins, *Symmetry classes of alternating sign matrices*, (2000); `arXiv:math.CO/0008045`.
69. D.P. Robbins and H. Rumsey, *Determinants and alternating-sign matrices*, Adv. Math. **62** (1986), 169–184.
70. H. Rosengren, *An Izergin-Korepin-type identity for the 8VSOS model, with applications to alternating sign matrices*, `arXiv:0801.1229`.
71. Yu. G. Stroganov, *The importance of being odd*, J. Phys. A **34** (2001), L179-L185; `arXiv:cond-mat/0012035`.
72. Yu. G. Stroganov, *A new way to deal with Izergin-Korepin determinant at root of unity* (2002); `arXiv:math-ph/0204042`.
73. B. Sutherland, *Exact solution of a two-dimensional model for hydrogen-bonded crystals*, Phys. Rev. Lett. **19** (1967), 103–104.
74. K. Szogo, *Toda molecule equation and quotient-difference method*, J. Phys. Soc. Japan **62** (1993), 1081–1084.

75. H. N. V. Temperley and E. H. Lieb, *Relations between the 'percolation' and 'colouring' problem and other graph-theoretical problems associated with regular planar lattices: some exact results for the 'percolation' problem*, Proc. R. Soc. London A **322** (1971), 251–280.
76. J. Thapper, *Refined counting of fully packed loop configurations*, Sem. Lothar. Combin. **56** (2006/07), Art. B56e, 27 pp.
77. A. Tsuchiya, *Determinant formula for the six-vertex model with reflecting end*, J. Math. Phys. **39** (1998), 5946–5951; `arXiv:solv-int/9804010`.
78. B. Wieland, *A large dihedral symmetry of the set of alternating sign matrices*, Electron. J. Combin. **7** (2000), R37; `arXiv:math/0006234`.
79. D. Zeilberger, *A fast algorithm for proving terminating hypergeometric identities*, Discr. Math. **80** (1990), 207–211.
80. D. Zeilberger, *The method of creative telescoping*, J. Symb. Comp. **11** (1991), 195–204.
81. D. Zeilberger, *Proof of the alternating sign matrix conjecture*, Electr. J. Combin. **3** (1996), R13.
82. D. Zeilberger, *Proof of the refined alternating sign matrix conjecture*, New York J. Math. **2** (1996), 59–68.
83. P. Zinn-Justin, *Six-vertex model with domain wall boundary conditions and one-matrix model*, Phys. Rev. E **62** (2000), 3411–3418; `arXiv:math-ph/0005008`.
84. P. Zinn-Justin, *Loop model with mixed boundary conditions, qKZ equation and Alternating Sign Matrices*, J. Stat. Mech. (2007), P01007; `arXiv:math-ph/0610067`.
85. J.-B. Zuber, *On the counting of fully packed loop configurations; some new conjectures*; Electr. J. Combin. **11** (2004), R13; `arxiv:math-ph/0309057`